Optics and Lasers in Engineering 169 (2023) 107692

Contents lists available at ScienceDirect

Optics and Lasers in Engineering

journal homepage: www.elsevier.com/locate/optlaseng

Video-rate quantitative phase imaging with dynamic acousto-optic defocusing

Christos Alexandropoulos [a], Martí Duocastella [a,b,*]

[a] Department of Applied Physics, Universitat de Barcelona, C/Martí i Franquès 1, Barcelona 08028, Spain
[b] Institut de Nanociència I Nanotecnologia (IN2UB), Av. Diagonal 645, Barcelona 08028, Spain

ARTICLE INFO

Keywords:
Varifocal lens
High-speed imaging
Quantitative phase microscopy
Weakly scattering samples

ABSTRACT

Various quantitative phase imaging techniques exist capable of characterizing transparent and low-contrast samples without the addition of dyes or fluorescent probes. Among them, the transport of intensity equation (TIE) allows phase retrieval by capturing information from different focal planes without complex inteferometric setups. However, current implementations can be limited in speed or accuracy by the lack of optical systems suitable for fast, reliable, and customizable focal plane selection. Here, we report how combining acousto-optics with pulsed illumination enables accurate and on-demand electronic defocus control suitable for TIE phase imaging at speeds only limited by the camera frame rate. The system exhibits diffraction-limited spatial resolution and high reconstruction fidelity, undistinguishable from traditional mechanical defocusing. We demonstrate its feasibility by measuring different dynamic events at rates as high as 100 phase maps per second. The tunability and ease of implementation of our system can pave the way to democratizing quantitative phase imaging in histopathology, fluid dynamics, and other fields involving thin transparent samples.

1. Introduction

One of the key challenges in optical microscopy is to rapidly extract quantitative information from a sample. Examples range from measuring the thickness of additively manufactured parts [1] to characterizing molecular diffusion inside a living cell [2]. These tasks can be successfully accomplished by state-of-the-art confocal and bright-field microscopes, but only with samples exhibiting a high optical contrast [3]. Indeed, existing microscope architectures are optimized to detect changes in the intensity of reflected, transmitted, or emitted light from a sample. However, many systems of interest such as histological slices, microlenses or in-vitro cell cultures consist of optically transparent objects with little or negligible contrast [4]. Even if staining solutions, fluorescent dyes or metallic coatings can be used to enhance optical contrast, these methods come at the expenses of increased sample preparation time, cost, and invasiveness [5].

Several techniques have been developed to address this issue and retrieve information from highly transparent samples. Among them, phase imaging methods offer high sample compatibility and the possibility of integration in most commercial microscopes, making them the preferred choice in most applications. Based on converting the phase delays that light experiences when interacting with optically transparent samples into intensity differences, they can be broadly classified into two groups depending on the information extracted from the sample. The first one includes techniques such as Phase Contrast Microscopy (PCM) [6] and Differential Interference Contrast (DIC) Microscopy [7]. As its name indicates, they enhance image contrast without retrieving quantitative information of the phase differences. The second group includes Quantitative Phase Imaging Techniques (QPI) such as interferometry, holography, and the Transport of Intensity Equation (TIE) [8]. They provide access to the local phase values of a sample, thus allowing quantifying parameters such as thickness or refractive index. Among QPI methods, TIE is particularly attractive given its ease of implementation, obviating the need for complex interferometers [9]. In particular, TIE solely requires two to three images, an in-focus and one or two defocused images, which are then used to computationally calculate the phase by solving an inverse problem.

Typically, the defocused images are captured by mechanical translation of sample or focusing optics along the axial direction [10–13]. While providing an on-demand selection of the focal planes of interest, this approach is limited by inertia, constraining the speed at which images can be acquired to some dozens of Hertz, insufficient for real-time phase imaging. Alternatively, it is possible to capture multiple defocused images in a single camera snaphot [14–16]. In this case, though, more complex optical instrumentation is required, its alignment is critical, and the defocus distances of the captured images are fixed [17] – note that the accuracy of the phase reconstruction depends on this parameter [9]. A strategy that can balance the trade-off between plane selection

* Corresponding author at: Department of Applied Physics, Universitat de Barcelona, C/Martí i Franquès 1, Barcelona 08028, Spain.
E-mail address: marti.duocastella@ub.edu (M. Duocastella).

https://doi.org/10.1016/j.optlaseng.2023.107692
Received 27 February 2023; Received in revised form 23 May 2023; Accepted 30 May 2023
0143-8166/© 2023 The Author(s). Published by Elsevier Ltd. This is an open access article under the CC BY-NC-ND license (http://creativecommons.org/licenses/by-nc-nd/4.0/)

and speed is to control the focus remotely. An example includes using electrically tunable lenses, but their response time is yet limited by mechanical deformation to hundreds of milliseconds [10]. Faster speeds are needed to study rapidly evolving biological systems or fast industrial processes. A promising method in this direction is the use of acousto-optical (AO) devices. Through the interaction of light with ultrasound, they can modulate, focus, and deflect a light beam with no mechanical elements at time scales as low as microseconds [18–20]. Still, the use of AO devices for quantitative phase imaging remains largely unexplored.

In this paper, we present an AO-enabled TIE system capable of retrieving quantitative phase information from a transparent sample at high speeds. Our microscope is based on the acousto-optic liquid lens TAG lens. As previously demonstrated, the TAG lens coupled with a microscope allows for the rapid collection of a z-stack [21,22]. We use such a unique ability to capture the information from the 3 focal planes needed for TIE at a speed only limited by the camera frame rate. We provide a detailed characterization of the optical resolution and reconstruction accuracy of our technique by imaging different test samples. As a proof of concept, we retrieve the phase information from different dynamic events, including an evaporating droplet, an in vitro cell, and a moving tissue section, at speeds as high as 100 reconstructions per second.

2. Principle of the AO-enabled tie microscope

The gist of our approach is the rapid acquisition of the information needed to solve the transport of intensity equation. Typically, a few images from different focal planes are sufficient. Indeed, the TIE relates the phase $\varphi(x, y)$ of an optical field at coordinates x, y to its intensity variations $\frac{\partial I\ (x,y)}{\partial z}$ along the propagation direction z as [23]:

$$-k\frac{\partial I(x,y)}{\partial z} = \nabla \cdot \ [I(x,y)\nabla\varphi(x,y)] \tag{1}$$

where $I(x, y)$ is the intensity distribution of an in-focus image, namely an image corresponding to an object located at the focal plane of the optical system, and k the wavenumber of the illumination source – note that partially coherent light provided from a light-emitting diode can be used [24,25]. Importantly, $\frac{\partial I\ (x,y)}{\partial z}$ can be estimated from two out-of-focus images $I_{+\Delta z}(x, y)$ and $I_{-\Delta z}(x, y)$ obtained, respectively, by moving the optical system relative to the sample an equal distance Δz above and below the focal plane:

$$\frac{\partial I(x,y)}{\partial z} \approx \frac{I_{+\Delta z}(x,y) - I_{-\Delta z}(x,y)}{2\Delta z} \tag{2}$$

Once $I(x, y)$ and $\frac{\partial I\ (x,y)}{\partial z}$ are known – only 3 images are necessary for this task– Eq. (1) can be numerically solved, and the phase map of an object can be retrieved (see Supplementary Information).

The robustness of the solution of the TIE, coupled with the high processing speed of current computers and high framerates of CMOS cameras, make this technique suitable for real-time quantitative phase imaging of thin and highly transparent samples. However, the challenge remains on how to capture the out-of-focus images rapidly and accurately. Note that, the ideal system should also provide tunable control of the defocus distance 2Δz. In fact, optimizing this parameter is key for reliable phase retrieval: for a too-large defocus distance, the low-frequency components of the images may be enhanced, resulting in blurred phase reconstructions; using a small 2Δz increases the error in the intensity derivative (see Eq. (2)), which can lead to reduced signal to noise ratio (SNR) and noisy phase reconstructions (see Supplementary Fig. S1).

The AO-enabled TIE microscope addresses this issue and offers an almost instantaneous control of the defocus distance, allowing for optimal Δz selection on any given object. As shown in Fig. 1, the core element of our system is an acousto-optic liquid lens, the TAG lens. It consists of a fluid-filled cylindrical piezoelectric cavity, that, when driven on resonance – 68 kHz in current experiments – induces a parabolic refractive index modulation in the fluid. Such constantly changing refractive index results in a varifocal lens whose optical power OP is given by [26]:

$$OP_{TAG}(t) = \frac{1}{f_{TAG}(t)} = A\omega^2 \sin(\omega t) \tag{3}$$

where f_{TAG} is the TAG lens focal length, A is a parameter that depends on the filling-fluid and piezoelectric properties, and ω the driving frequency. When placed at a conjugate plan of the back focal plane of a microscope objective with focal length f_{obj}, the changes in the OP of the TAG lens result in a continuous shift of the focal plane of the objective given by:

$$\Delta z(t) = \frac{f_{obj}^2}{f_{TAG}(t)} \tag{4}$$

where we have assumed unit magnification in the relay system between objective and TAG lens. Because the focal plane of the system is periodically scanned at about 15 μs, a speed much faster than the integration time of any camera detector, we used synchronized pulsed illumination. Specifically, we use trains of 400 ns pulses at three different time delays with respect to the focal sweeping, each resulting in the acquisition of an image at a different focal plane (see Materials and Methods). Therefore, by controlling these time delays, we have the freedom to select any three focal planes within the z-scanned range. This provides our system with an on-demand control of the defocus distance, and hence with the ability to capture the optimal three images necessary for accurate phase retrieval with TIE.

3. Results

3.1. Image quality and spatial resolution

Initially, we compared the electronic focus control of our AO-enabled microscope with the traditional approach based on mechanical sample translation. To this end, we captured a series of images of a USAF target at different focal positions of our microscope (Fig. 1b). Notably, the images captured by mechanically defocusing the sample over an axial range of 50 μm look identical to those acquired by keeping the sample at the focal plane and using the TAG lens for electronic defocusing. For a quantitative assessment of the similarity between the two methods, we employed the structural similarity index (SSI). Fig. 1c shows the plot of this value for the different axial positions interrogated. In agreement with the qualitative perception, all images exhibit an SSI value of around 98%, very close to the 100% value that corresponds to identical images.

We performed a more refined analysis of the optical performance of our AO-enabled microscope by using Fourier Ring Correlation (FRC). This method offers direct access to the spatial resolution of an optical system for a given signal-to-noise ratio (SNR). As shown in Fig. 2a, at high SNR conditions – exposure time of 24 ms and 41 fps – the maximum spatial resolution of the system is about 1 μm for both electronic and mechanical z-scanning. This value is in agreement with the 0.95 μm corresponding to the diffraction limit of the 0.30 NA objective used. As expected, the spatial resolution progressively decreases with the out-of-focus distance. Therefore, not only the integration of the TAG lens into a commercial microscope preserves the system's optical resolution, but electronic focus control is found again to be indistinguishable from mechanical sample translation.

Increasing the imaging speed of our system can be achieved by reducing the camera exposure time. In this case, a reduction in SNR is also expected, especially for biological samples where high light intensities – that would help to otherwise compensate for the loss of signal - can lead to photodamage. To better characterize the spatial resolution of our system at these low SNR conditions, we used again FRC at exposure times of 8 and 3 ms, corresponding to 125 and 300 fps, respectively, while maintaining the same light intensity. The overall resolution of the system slightly decreases with the camera frame rate, and the noisier the images, the higher the uncertainty in the evaluation of the resolution (Fig. 2a). Still, the same trends observed for the high SNR case

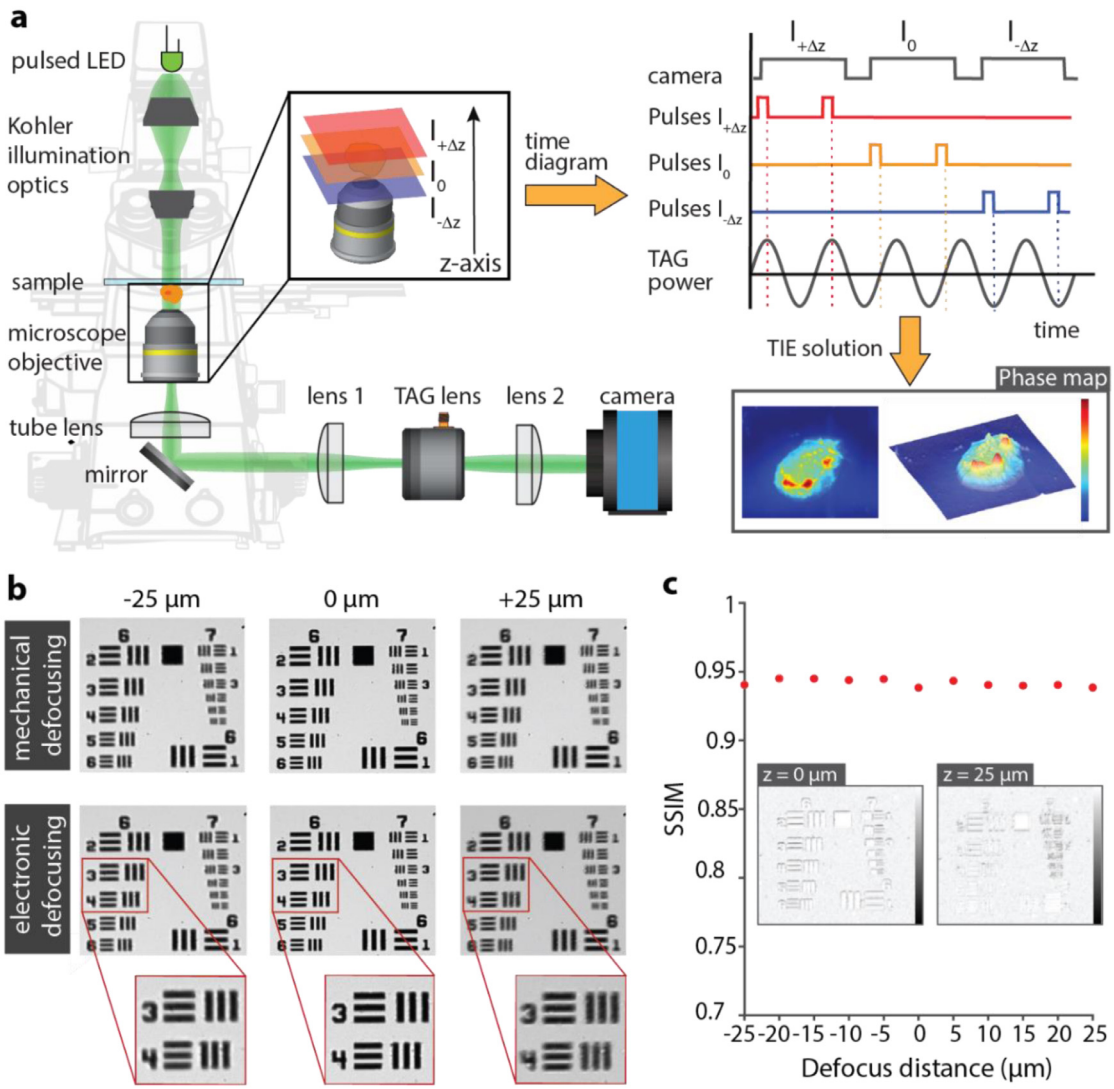

Fig. 1. Principle of electronic defocusing with an acousto-optic lens. (a) Scheme of the AO-enabled TIE microscope and the timing diagram. (b) Optical micrographs of a USAF target at different axial positions (−25,0 and +25um), captured using AO-enabled electronic defocusing and traditional mechanical stage translation. The line width of the group 6, element 3 of the target is 6.2 µm. (c) Plot of the similarity values at different axial positions between images captured with electronic and mechanical defocusing. The insets correspond to the SSIM index maps at the focal plane (0 µm) and at a defocused position (25 µm). The white pixels correspond to areas with no differences between electronic and acousto-optic defocusing.

remain valid, that is, the progressive deterioration in resolution as the images get defocused, and the good agreement between electronic and mechanical axial focus control.

3.2. Reconstruction fidelity

The above results show promise toward the use of the AO-enabled microscope for phase retrieval using the TIE. To confirm it, we evaluated the fidelity of the phase reconstructions using electronic focus translation. In particular, we employed a microlens with known refractive index and size as our reference sample. Fig. 2b shows three images of the microlens at the focal plane of the microscope and 20 µm above and below it, together with the reconstructed phase map. The latter exhibits a circular shape with a continuous phase gradient, consistent with the microlens shape. For a more precise quantification, we converted the phase values at a given position $\varphi(x, y)$ into the corresponding microlens thickness $d(x, y)$ by using the relationship between optical path difference and phase:

$$d(x, y) = \frac{\lambda\, \varphi(x, y)}{2\pi\left(n_l - n_o\right)} \tag{5}$$

where λ is the wavelength of the illumination source, and n_l and n_o are the refractive index of the microlens and surrounding medium (air in experiment herein), respectively. As shown in Fig. 2c, the retrieved thickness map is in excellent agreement with that measured using a commercial 3D confocal optical profilometer (Sensofar S Neox 090), that is, the gold standard optical metrology tool. A topography line profile through the microlens center reveals a difference of about 10% between the two methods (Fig. 2c). Remarkably, such a high level of accuracy is maintained as the acquisition speed increases, with the line profiles acquired at 125 and 333 fps exhibiting discrepancies of only 9 and 13% with respect to the confocal profile, respectively. These acquisition speeds cannot be achieved with commercial confocal microscopes, where the need for axial scanning limits their capacity for the 3D characterization of rapidly evolving processes to some dozens of frames per second [27].

3.3. Dynamic phase imaging

The good reconstruction fidelity and imaging speed of our AO-enabled TIE microscope opens the door to characterize transparent objects in motion or rapidly evolving. A paradigmatic example is that of

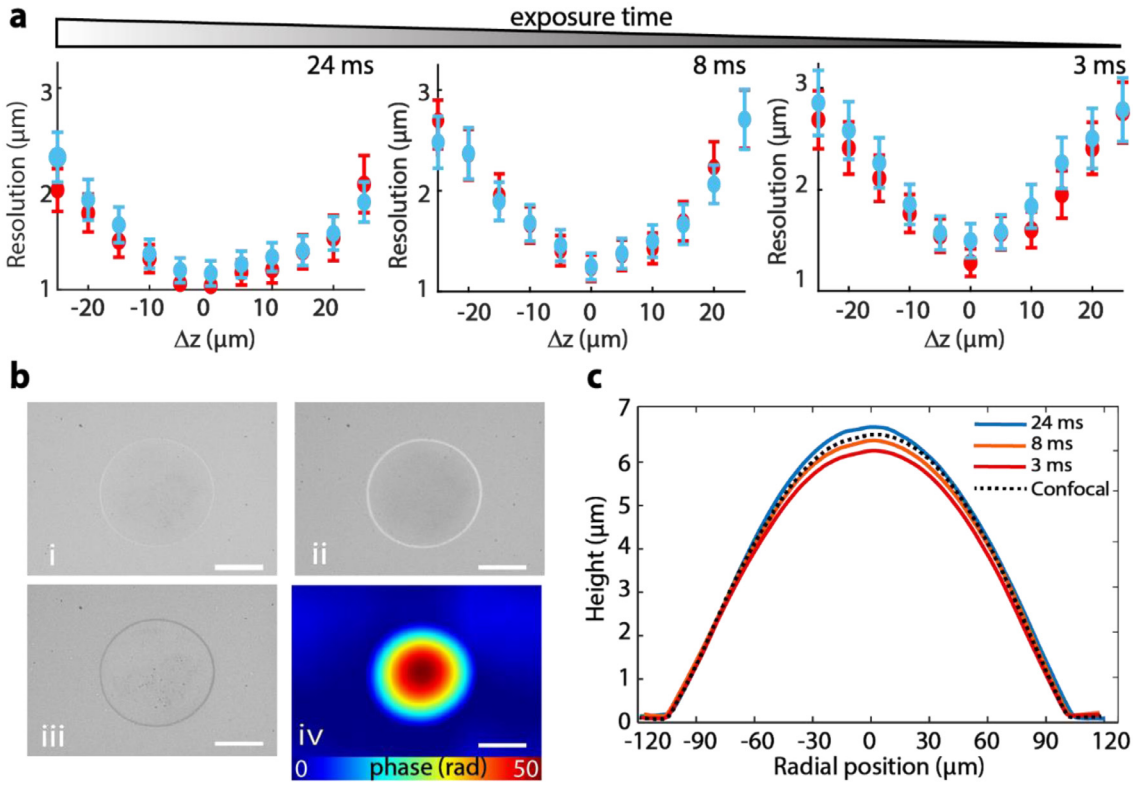

Fig. 2. AO-enabled microscope spatial resolution and TIE reconstruction fidelity. (a) Plot of the spatial resolution of the microscope versus focus position at different exposure times measured using FRC. Blue and red dots correspond to measurements obtained with AO-enabled electronic and traditional mechanical focus translation, respectively. (b) Brightfield images of the microlones in-focus (i), defocused 20 μm above the focal plane (ii) and defocused 20 μm below the focus. (iv) Phase map reconstructed with TIE. Scale bars 100 μm. (c) Height profile lines of the microlens at different camera exposure times (24,8,3 ms) using the same Δz. An optical confocal measurement is included for comparision.

an evaporating water droplet. The kinetics of this phenomenon play an important role in relevant applications varying from surface modification [28] to tissue engineering [29], which has spurred a myriad of theoretical and experimental studies. Typically, experimental realizations assume the droplet to be a spherical cap, and by using a goniometer and an image acquisition system, the droplet volume is calculated over time [30]. However, this approach is difficult to adapt for small droplets and cannot cope with irregular droplets. These issues can be addressed by our microscope, which allows direct extraction of the droplet volume at a given time instance. To prove this point, we imaged a water microdroplet with a base radius of 110 μm placed on top of a glass slide, with an initial volume of 1.86 nL. Note that this volume is about 3 orders of magnitude smaller than that used in conventional studies. The experiment was performed at 22 °C. By the sequential capture of the three images required to solve the TIE (with Δz equal to ±40 μm) at 320 fps, we gathered the phase maps of the evaporating droplet at an impressive rate of 106 reconstructions per second (Fig. 3a). This speed is about 10 times faster than traditional methods.

Fig. 3b shows the plot of the evolution of the microdroplet volume versus time. Notably, we made no assumptions regarding the shape or size of the droplet in our measurements. Because the refractive index of water and the wavelength of the illumination light are known, the phase measurements of the AO-enabled TIE microscope can be directly converted into a thickness map (Eq. (5)). A simple integration of the thickness map, provided the pixel size is known, leads to the calculation of the droplet volume over time. During the first 7 s of the evaporation process, there is pinning of the contact line, and thus the microdroplet height progressively decreases while maintaining a fixed base radius. This behavior can be clearly observed in Supplementary Video 1 and Fig. 3c.

A linear fit of these initial time points enables calculation of the evaporation rate. The slope of the fitted line is equal to 0.14 nL/s which is in great accordance with the values of experiments previously reported for pinned droplets [30,31]. After this initial stage, the microdroplet continues to evaporate, but pinning is lost. The volume change is no longer linear with time, until at, about 14 s after measurements are initiated, the microdroplet is fully evaporated. Interestingly, this regime is typically inaccessible with conventional measurement methods. Thus, our system is capable of characterizing the physics of liquid evaporation on irregular substrates and other less constrained environments.

3.4. Phase reconstruction of biological samples

To further test the capabilities of our system, we retrieved the phase information of an unstained biological sample. Arguably, it is in characterizing this type of intrinsically low-contrast and delicate objects where the TIE offers the most advantages [9,11,32–34]. In this case, we first reconstructed the phase map of an isolated cheek cell collected with a cotton swab and placed on a microscope glass slide in open air without any additional preparation. Fig. 4a shows the in-focus image and one of the two defocused images required to solve the TIE, together with the retrieved phase information. Acquisition was performed at a remarkable speed of 200 fps, which allows averaging for enhanced SNR. As expected, the in-focus brightfield image does not provide enough contrast to discriminate the cell's structural characteristics. Instead, the phase map allows distinguishing not only the cell's boundaries from the background but also subcellular structures. This result validates the usage of our microscope for quantitative phase imaging in life sciences applications.

The high-speed of the AO-enabled TIE microscope can be used to perform tasks not possible with current phase imaging systems. As a

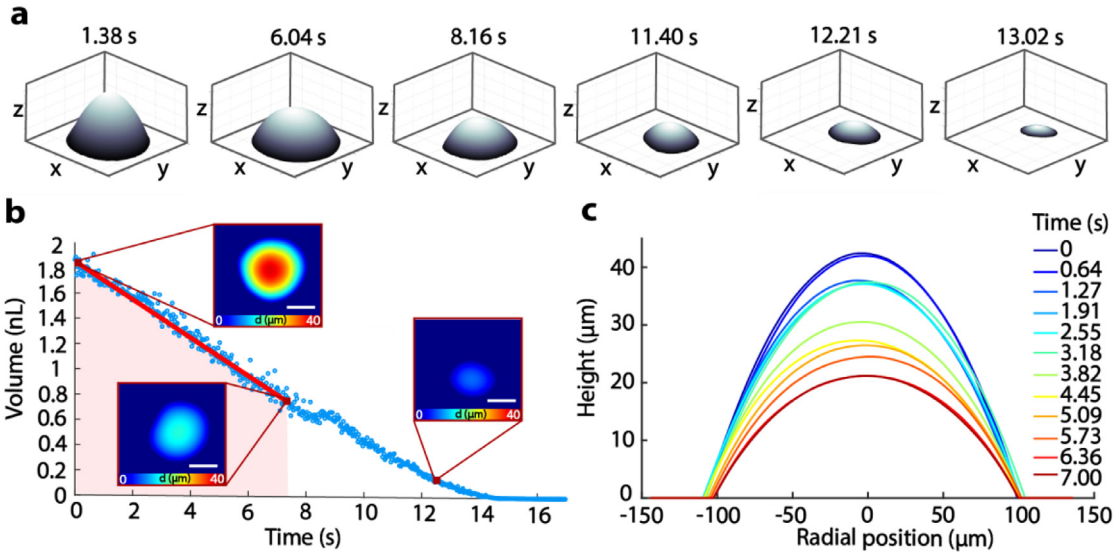

Fig. 3. Phase imaging of the dynamics of an evaporating water microdroplet. (a) Thickness map reconstructions of the evaporating microdroplet at different time instances. The x-y-z box size is 400×400×45 μm. (b) Plot of the microdroplet volume over time. The insets correspond to the measured phase maps of the microdroplets at different time instances. During the first 7 s, there is pinning of the microdroplet contact line, and the evaporation rate can be calculated by a linear fit (solid red line). Scale bars 100 μm. (c) Topographic line profiles along the microdroplet center during pinning.

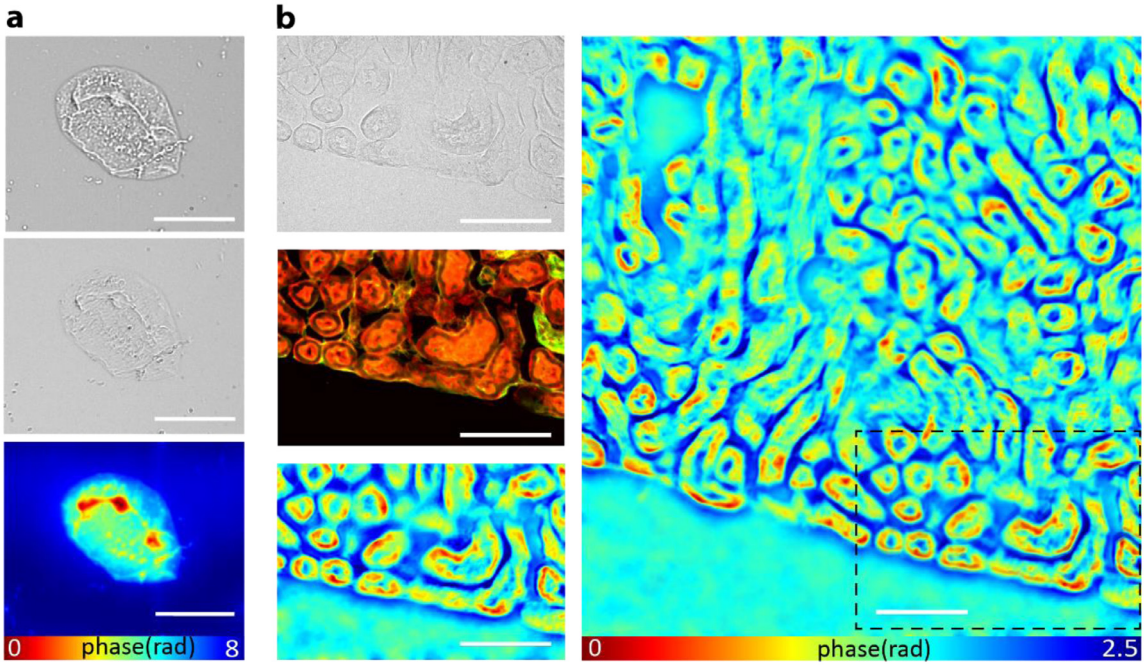

Fig. 4. Phase Reconstruction of biological samples. (a) From top to bottom: defocus (+10um) and in-focus brightfield images of a cheek cell, and the corresponding phase map reconstructed with the AO-enabled TIE microscope. Scale bars 100 μm. (b) Left column, from top to bottom: in-focus brightfield image, fluorescence image, and phase reconstruction of a mouse kidney section. Right: extended Field of View phase map obtained by stitching several phase reconstructions. The dashed black square corresponds to the camera field of view. Scale bars 100 μm.

proof-of-concept, we combined the TIE phase retrieval method with manual sample translation and image stitching to obtain a phase map of a large area of a 16 μm mouse kidney section (FluoCells Prepared Slide #3, ThermoFisher Scientific). Such a combination can help leverage the intrinsic trade-off between spatial resolution and field of view of microscopes, providing access to detailed information over large areas. Supplementary Video 2 shows the reconstructed phase maps during the manual movement of the sample along the x and y axis. We were able to capture the 3 images needed for TIE at a camera frame rate of 200 fps. This represents a striking speed of 66 phase maps per second, that is, above video-rate phase imaging. At each position, the internal differences of the kidney tissue are clearly discernible, in contrast to a bright-field image of the same region, as shown in Fig. 4a. A comparison with a fluorescence image is also illustrated in the same figure.

In this case, the red channel represents the filamentous actin prevalent in glomeruli and the brush border, while the green one is the glomeruli and convoluted tubules of the kidney. Both fluorescence and phase map images exhibit a very high contrast and sub-cellular spatial resolution. The largest difference between the two lies on the high specificity of fluorescence, inexistent in quantitative phase imaging tech-

niques. Note, though, that recent advances in artificial intelligence are narrowing the gap between these techniques, and after appropriate training, one can now virtually stain phase images with results similar to those achieved with fluorescence [35].

From the phase maps corresponding to different sample regions, we can reconstruct a stitched image covering a large field of view. Interestingly, by using the latest developments in image stitching algorithms, no prior knowledge of the exact position coordinates of the captured frames is required [36]. Indeed, we simply moved the sample manually for about 5 s, fed the reconstructed phase maps to the stitching algorithm, and obtained an extended field of view image (Fig. 4b). The overall region covers an area more than 6x that of an individual phase map, but it could be drastically increased by either moving the sample for a longer time or moving it faster, for instance, by using a high-speed XY motorized stage. Note that, as the number of collected images increases, the image stitching process can become computationally expensive [37]. Still, significant progress has been made in this front to improve speed and stitching efficiency through feature selection, deep learning, and parameter optimization [38]. Combined with fast processors such as graphical processing units (GPUs), it is possible today to perform image stitching in real time [39]. Therefore, AO-enabled TIE is a promising technique for the high-resolution label-free imaging of large histopathology sections.

4. Conclusions

The combination of an acousto-optic liquid lens with a commercial bright-field microscope and synchronized pulsed illumination enables quantitative phase measurements at high speeds. The electronic focus control provided by such a system is indistinguishable from traditional mechanical z-scanning, providing on-demand access to the information needed for solving the transport of intensity equation. As our results demonstrate, phase maps of dynamics events at micrometric resolution can be precisely characterized at more than 100 reconstructions per second, only limited by the camera frame rate.

The high speed and tunability of our system makes it suitable for optimal and high throughput extraction of information from transparent and low-contrast samples. Its ease of implementation and reduced processing time – compatible with the computational units of commercial laptops – allows imaging over user-selectable areas, beyond the field of view limit imposed by the particular optics used. We anticipate that our approach will help to democratize the transport of intensity equation as a real-time phase imaging tool in fields as relevant as fluid mechanics and histopathology.

5. Materials and methods

5.1. Optical setup

The core elements of the AO-enabled TIE system consist of an inverted brightfield microscope (Nikon ECLIPSE Ti2 Series) with a 10x, 0.3 NA objective lens (Nikon LU Plan Fluor), an off-the shelf green color LED with a central wavelength of 550 nm (Nichia LED, NSPE510DS) mounted at the lamphouse port of the microscope (transmission mode), a 4f system consisting of two lenses of 200 mm focal length, with the TAG lens (TAG lens 2.0, TAG Optics, Inc.) placed in between, and a monochrome camera (The Imaging Source, DMK 33UX287). The 4f system was placed at the left port of the microscope, as shown in Fig. 1a. To ensure an even illumination of the sample across the entire field of view of the microscope, we included a Köhler illumination system consisting of a collector lens, a field lens, and a condenser lens.

To drive the TAG lens, we used a signal with a frequency of $f_{TAG} \approx 69\,kHz$ and amplitude voltage of 20 V generated with an arbitrary waveform generator (BK PRESISION, 4053B Series). In this configuration, the TAG lens provides an axial scan range of 100 μm. The LED was driven with the signal from the output of a pulse delay generator (QUANTUM COMPOSERS, 9520 Series) synchronized with the TAG lens. Specifically, three different trains of pulses were sent to the LED. Each train contained pulses with a duration of 400 ns and amplitude voltage of 7 V, and whose number was approximately given by t_{camera}/f_{TAG}, where t_{camera} is the camera exposure time. The pulses in each train had the same frequency as the TAG lens driving signal but with a different phase delay. By controlling the phase delay of the trains, we could precisely select the defocus distance – for each experiment, we selected the phase delay that corresponded to the desired defocus distances for solving the TIE. In addition, the same pulse delay generator was used to deliver the trigger signal for the camera at the beginning of each train. Note that by using a train of pulses instead of a single pulse, we drastically enhanced SNR.

5.2. FRC measurements

We performed the FRC analysis using images from a Resolution target (Photomask Portal RTΔ39D22 434 nm). In more detail, we used 11 images at each axial position where the resolution was to be determined. We then computed the FRC for the 55 different possible combinations of image pairs using the algorithm adopted from [40]. By adopting the 0.1 threshold criterion, we extracted for each FRC the cut-off frequency and, consequently, the maximum spatial resolution of the system (see Supplementary Information). The average and standard deviation of the 55 calculated values represented the final maximum spatial resolution and error, respectively, at a given axial position. We repeated this process for 3 different camera exposure times (24,8 and 3 ms) across an axial range of 50 μm, in steps of 5 μm, using the electronic focus control enabled by the TAG lens and traditional mechanical defocusing.

5.3. TIE solver

In all experiments we adopted a fast Fourier transform (FFT) based solver to compute the solution of the TIE. Such a method is well-adopted in the literature for its high speed and computational efficiency [41]. The inputs of the solver are the in-focus image, the two defocused images for the intensity derivative calculation, the defocus distance 2Δz, the pixel size of the camera, and the wavelength λ. It is also necessary to use a minimum intensity threshold parameter, to prevent the division with zero when the in-focus image intensity values are very small as it is described in [41]. To determine the optimal defocus distance for each object to be characterized, we selected criteria proposed by [42], based on the object spatial spectrum and the noise characteristics of the detector.

5.4. Fluorescence imaging and image stitching

The addition of the TAG lens to the commercial Nikon Eclipse Ti2 does not preclude its normal use in reflection or fluorescence mode. Thus, we employed the included fluorescence illuminator (X-Cite 120LEDmini LED Illumination System, Excelitas Technologies) at 40% of its maximum illumination power to capture two sequential fluoresce images using the (Semrock, Brightline, Ex: 554/23, Em: 609/54, Di: 573 nm) green/red and (Ex: 466/40, Em: 525/50, Di: 495 nm) blue/green filter cubes, respectively. The two grayscale images were artificially coloured using ImageJ to red and green, respectively, and merged to produce the final composite fluorescent image.

5.5. Image processing

The implementation of the TIE solver and all image processing was performed in a regular desktop computer featuring an Intel Corei7 processor (10700 CPU @ 2.90 Ghz) and 16GB RAM. All algorithms, including the FFT-based solver and FRC, were implemented using MATLAB.

Declaration of Competing Interest

The authors declare the following financial interests/personal relationships which may be considered as potential competing interests:

CRediT authorship contribution statement

Christos Alexandropoulos: Methodology, Investigation, Validation, Writing – original draft. **Martí Duocastella:** Conceptualization, Methodology, Writing – review & editing, Supervision, Funding acquisition.

Data availability

Data will be made available on request.

Acknowledgments

This work was supported by the EU-funded OrganVision Horizon 2020 project, Grant agreement number 964800. We thank Dr. Andrea Marchese from Universitat de Barcelona and Prof. Peter Saggau from Baylor College of Medicine for useful discussions. M.D. is a Serra Hunter professor.

Supplementary materials

Supplementary material associated with this article can be found, in the online version, at doi:10.1016/j.optlaseng.2023.107692.

References

[1] Agour M, Riemer O, Flosky C, Meier A, Bergmann RB, Falldorf C. Quantitative phase contrast imaging of microinjection molded parts using computational shear interferometry. IEEE Trans Ind Inform 2016;12:1623–30.
[2] Robson A, Burrage K, Leake MC. Inferring diffusion in single live cells at the single–molecule level. Philos Trans R. Soc B Biol Sci 2013;368.
[3] Nwaneshiudu A, Kuschal C, Sakamoto FH, Rox Anderson R, Schwarzenberger K, Young RC. Introduction to confocal microscopy. J Invest Dermatol 2012;132: 1–5.
[4] Doblas A, Sánchez-Ortiga E, Martínez-Corral M, Saavedra G, Garcia-Sucerquia J. Accurate single-shot quantitative phase imaging of biological specimens with telecentric digital holographic microscopy. J Biomed Opt 2014;19:046022.
[5] Rivenson Y, Wang H, Wei Z, de Haan K, Zhang Y, Wu Y, Günaydın H, Zuckerman JE, Chong T, Sisk AE, Westbrook LM, Wallace WD, Ozcan A. Virtual histological staining of unlabelled tissue-autofluorescence images via deep learning. Nat Biomed Eng 2019;3:466–77.
[6] Centonze Frohlich V. Phase contrast and differential interference contrast (DIC) microscopy. J Vis Exp 2008(17):844.
[7] Stender AS, Marchuk K, Liu C, Sander S, Meyer MW, Smith EA, Neupane B, Wang G, Li J, Cheng JX, Huang B, Fang N. Single cell optical imaging and spectroscopy. Chem Rev 2013;113:2469–527.
[8] Park YK, Depeursinge C, Popescu G. Quantitative phase imaging in biomedicine. Nat Photonics 2018;12:578–89.
[9] Zuo C, Li J, Sun J, Fan Y, Zhang J, Lu L, et al. Transport of intensity equation: a tutorial. Opt Lasers Eng 2020;135:2–20.
[10] Zuo C, Chen Q, Qu W, Asundi A. High-speed transport-of-intensity phase microscopy with an electrically tunable lens. Opt Express 2013;21:24060.
[11] Yu W, Tian X, He X, Song X, Xue L, Liu C, et al. Real time quantitative phase microscopy based on single-shot transport of intensity equation (ssTIE) method. Appl Phys Lett 2016;109:071112.
[12] Zuo C, Sun J, Li J, Zhang J, Asundi A, Chen Q. High-resolution transport-of-intensity quantitative phase microscopy with annular illumination. Sci Rep 2017;7:1–22 2017 71.
[13] Petruccelli JC, Chakraborty T. Source diversity for transport of intensity phase imaging. Opt Express 2017;25(8):9131–2.
[14] Waller L, Yang SY, Barbastathis G, Luo Y. Transport of intensity phase imaging in a volume holographic microscope. Opt Lett 2010;35(17):2961–3.
[15] Di Martino JM, Ayubi GA, Dalchiele EA, Alonso JR, Fernández A, Flores JL, Perciante CD, Ferrari JA. Single-shot phase recovery using two laterally separated defocused images. Opt Commun 2013;293:1–3.
[16] Hai N, Kumar R, Rosen J. Single-shot TIE using polarization multiplexing (STIEP) for quantitative phase imaging. Opt Lasers Eng 2022;151:106912.
[17] Picazo-Bueno JA, Micó V. Optical module for single-shot quantitative phase imaging based on the transport of intensity equation with field of view multiplexing. Opt Express 2021;29:39904.
[18] Duocastella M, Surdo S, Zunino A, Diaspro A, Saggau P. Acousto-optic systems for advanced microscopy. J Phys Photonics 2021;3(1):3–6.
[19] Szulzycki K, Savaryn V, Grulkowski I. Rapid acousto-optic focus tuning for improvement of imaging performance in confocal microscopy. Appl Opt 2018;57:C14.
[20] Zunino A, Garzella F, Trianni A, Saggau P, Bianchini P, Diaspro A, et al. Multiplane encoded light-sheet microscopy for enhanced 3D imaging. ACS Photonics 2021;8(11):3385–90.
[21] Kang SK, Duocastella M, Arnold CB. Variable optical elements for fast focus control. Nat Photon 2020;14:533–42.
[22] Duocastella M, Vicidomini G, Diaspro A. Simultaneous multiplane confocal microscopy using acoustic tunable lenses. Opt Express 2014;22:19293.
[23] Teague MR. Irradiance moments: their propagation and use for unique retrieval of phase. J Opt Soc Am 1982;72:1199–209 V.
[24] Barbastathis G, Petruccelli JC, Tian L. The transport of intensity equation for optical path length recovery using partially coherent illumination. Opt Express 2013;21(12):14430–41 **21**14430–14441.
[25] Roberts A, Nugent KA, Gureyev TE. Partially coherent fields, the transport-of-intensity equation, and phase uniqueness. JOSA A 1995;12(9):1942–6 **12**1942–1946.
[26] Duocastella M, Sun B, Arnold CB. Simultaneous imaging of multiple focal planes for three-dimensional microscopy using ultra-high-speed adaptive optics. J Biomed Opt 2012;17(5):050505.
[27] Deguchi T, Bianchini P, Palazzolo G, Oneto M, Diaspro A, Duocastella M. Volumetric Lissajous confocal microscopy with tunable spatiotemporal resolution. Biomed Opt Express 2020;11:6293.
[28] Haschke T, Wiechert W, Graf K, Bonaccurso E, Li G, Suttmeier FT. Evaporation of solvent microdrops on polymer substrates: From well controlled experiments to mathematical models and back. Nanoscale Microscale Thermophys Eng 2007;11(1–2):31–41.
[29] Zang D, Tarafdar S, Tarasevich YY, Choudhury MD, Dutta T. Evaporation of a droplet: from physics to applications. Phys Rep 2019;804:1–56.
[30] Dunn GJ, Wilson SK, Duffy BR, David S, Sefiane K. The strong influence of substrate conductivity on droplet evaporation. J Fluid Mech 2009;623:329–51.
[31] Hu H, Larson RG. Evaporation of a sessile droplet on a substrate. J Phys Chem B 2002;106:1334–44.
[32] Zhang J, Zhang J, Zhang J, Chen Q, Chen Q, Chen Q, Sun J, Sun J, Sun J, Tian L, Tian L, Zuo C, Zuo C, Zuo C, Zuo C. On a universal solution to the transport-of-intensity equation. Opt Lett 2020;45(13):3649–52 **45**3649–3652.
[33] Poola PK, John R. Label-free nanoscale characterization of red blood cell structure and dynamics using single-shot transport of intensity equation. J Biomed Opt 2017;22:1.
[34] Li Y, Di J, Ma C, Zhang J, Zhong J, Wang K, Xi T, Zhao J. Quantitative phase microscopy for cellular dynamics based on transport of intensity equation. Opt Express 2018;26:586.
[35] Somani A, Sekh AA, Opstad IS, Birgisdottir ÅB, Myrmel T, Ahluwalia BS, et al. Virtual labeling of mitochondria in living cells using correlative imaging and physics-guided deep learning. Biomed Opt Express 2022;13:5508–14.
[36] Preibisch S, Saalfeld S, Tomancak P. Globally optimal stitching of tiled 3D microscopic image acquisitions. Bioinformatics 2009;25:1463–5.
[37] Chalfoun J, Majurski M, Blattner T, Bhadriraju K, Keyrouz W, Bajcsy P, Brady M. MIST: accurate and scalable microscopy image stitching tool with stage modeling and error minimization OPEN. Sci Rep 2017;7:4988.
[38] Suman S, Rastogi U, Tiwari R. Image stitching algorithms-a review. Circ Comput Sci 2016;1:14–18.
[39] Tennoe M, Helgedagsrud E, Naess M, Alstad HK, Stensland HK, Gaddam VR, Johansen D, Griwodz C, Halvorsen P. Efficient implementation and processing of a real-time panorama video pipeline. In: Proceedings of the IEEE international symposium on multimedia, ISM; 2013. p. 76–83. 2013.
[40] Diederich B, Then P, Jügler A, Förster R, Heintzmann R. cellSTORM - Cost-effective super-resolution on a cellphone using dSTORM. PLoS One 2018;14:1–2.
[41] Zhang J, Chen Q, Sun J, Tian L, Zuo C. On a universal solution to the transport-of-intensity equation. Opt Lett 2020;45:3649.
[42] Waller L, Barbastathis G, Tian L. Transport of Intensity phase-amplitude imaging with higher order intensity derivatives. Opt Express 2010;18(12):12552–61 **18**12552–12561.